Angewandte Communications

Oxygen Evolution

DOI: 10.1002/anie.201((will be filled in by the editorial staff))

Graphitic Carbon Nitride Nanosheet-Carbon Nanotube Three-Dimensional Porous Composites as High-Performance Oxygen Evolution Electrocatalysts**

*Tian Yi Ma, Sheng Dai, Mietek Jaroniec and Shi Zhang Qiao**

***Abstract**: A new class of highly efficient oxygen evolution catalysts is synthesized through self-assembly of ultrathin graphitic carbon nitride nanosheets (g-C_3N_4 NSs) and carbon nanotubes (CNTs), driven by π-π stacking and electrostatic interactions. Remarkably, they exhibit higher catalytic oxygen evolution activity and stronger durability than Ir-based noble metal catalysts, and display the best performance among reported non-metal catalysts, which is attributed to the high nitrogen content, efficient mass and charge transfer in the porous three-dimensional nanostructure.*

Design of highly active and stable catalysts for oxygen evolution reaction (OER) is urgently needed because OER is the efficiency-limiting process for many important electrochemical energy conversion devices such as metal-air batteries and fuel cells,[1] and the most efficient catalysts for the sluggish OER are still noble metals, *i.e.* Ir and Ru-based materials.[2] To replace expensive Ir and Ru, numerous efforts have been undertaken toward using transition-metal alternatives (Co, Fe, Mn, *etc.*),[3] in which metal species are considered to be the active sites. However, the complicated fabrication procedure and the low conductivity of metal oxides largely limit their applications, which in the most cases underperform noble metal catalysts. In contrast to the metal-based catalysts, the non-metal OER catalysts consisting of less expensive earth-abundant elements (C, H, O, N) that are also the building elements of the active species formed during processing these OER catalysts, are rarely reported. Only a few reports are devoted to N-active materials including organic N(5)-ethylflavinium ions[4] and N-doped graphene/carbon nanotube composites,[5] but their catalytic activity is still unsatisfactory. A recent breakthrough was achieved by synthesizing N-doped graphitic carbon materials (N/C), which afforded a 10 mA cm^{-2} current density at 1.61 V *vs.* reversible hydrogen electrode (RHE),[6] approaching that of IrO_2/C. The pyridinic and quaternary N atoms were proven to be the active sites for OER, similar to the reverse oxygen reduction reaction (ORR) catalyzed by N doped carbon materials;[7] however, in this case Ni species were added in the preparation process to graphitize the N/C catalysts. Despite some drawbacks, these efforts inspire us to seek N-rich and highly conductive (graphitic) carbon materials that are able to efficiently catalyze OER.

Carbons with doped N can greatly improve the stability of the resultant catalysts due to an enhanced π bonding in the framework, and promote their electron donor-acceptor property, consequently enhancing their catalytic activity for specific electrochemical reactions.[7] Among various precursors, the graphitic carbon nitride (g-C_3N_4) is especially promising for introducing N into carbon materials, due to its high N content, low cost, and easily tailorable structure;[8] however, scarce efforts have been made to employ g-C_3N_4 as the active species for electrocatalytic OER. The optimal use of g-C_3N_4 for electrochemical applications requires the improvement of its poor conductivity. Generally, two types of methods have been applied, *i.e.* physical mixing of g-C_3N_4 with conductive carbons[9] and *in situ* immobilization of g-C_3N_4 onto carbon supports.[7b,d,10] The poor contact and inhomogeneity between physically mixed g-C_3N_4 aggregates and carbon is the major disadvantage for the former method; while for the latter route, the high-temperature polymerization (≥ 500 °C) of monomers (*e.g.* dicyandiamide and melamine) to produce g-C_3N_4 inside the carbon matrix may undesirably lead to the substantial reduction of the N content. Thus, a better fabrication strategy that assures a strong interaction between g-C_3N_4 and carbon supports at relatively low temperatures is highly desirable. Recently, two-dimensional (2D) ultrathin g-C_3N_4 nanosheets (g-C_3N_4 NSs) were synthesized by de-stacking the layered bulk g-C_3N_4 through thermal oxidation etching[11] and liquid exfoliation.[12] Although these two strategies still suffer from extremely low yield and long sonication time (10–16 h), respectively, the opening of interlayer space in this layered material enlarges its surface area, which is promising for improving its interaction with other substances (*e.g.* carbon) and reactants, and consequently, for enhancing its electrical and chemical properties as compared to the bulk counterpart.

Here we report a facile low-temperature self-assembly of ultrathin g-C_3N_4 NSs and carbon nanotubes (CNTs) to obtain the strongly coupled composite OER catalysts (denoted as g-C_3N_4 NS-CNT). The utilization of g-C_3N_4 NSs as the precursor instead of bulk g-C_3N_4 facilitates the robust assembly to form a three-dimensional (3D) interconnected network, which possesses a well-developed porous structure with large surface area (149 m^2 g^{-1}) and high N content (23.7 wt.%). These electrocatalysts display better activity and stronger durability than the nano-sized IrO_2 catalyst supported on CNTs (denoted as IrO_2-CNT; for synthesis details see Supporting Information).

[*] Dr. T. Y. Ma, A/Prof. S. Dai, Prof. S. Z. Qiao
School of Chemical Engineering
The University of Adelaide, Adelaide, SA 5005 (Australia)
E-mail:s.qiao@adelaide.edu.au

Prof. M. Jaroniec
Department of Chemistry and Biochemistry
Kent State University, Kent, Ohio 44240 (USA)

[**] This work is financially supported by the Australian Research Council (ARC) through the Discovery Project programs (DP140104062 and DP130104459).

Supporting information for this article is available on the WWW under http://dx.doi.org/10.1002/anie.201xxxxxx.

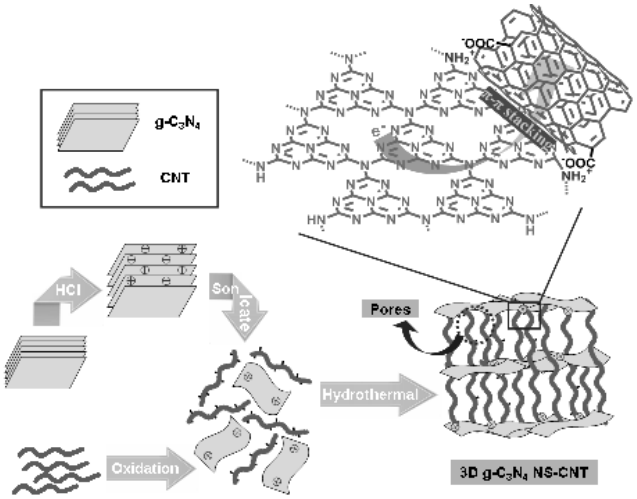

Scheme 1. Fabrication of 3D g-C_3N_4 NS-CNT porous composite.

Ultrathin 2D g-C_3N_4 NSs were first prepared by sonication-exfoliation of protonated g-C_3N_4 (**Scheme 1**). The protonation was conducted by using concentrated hydrochloric acid, which not only efficiently reduced the subsequent exfoliation time to ~2 h (*vs.* 10–16 h without protonation[12]) due to the disruption of the interplanar and in-planar cohesion in the bulk g-C_3N_4 (*e.g.* van der Waals forces and hydrogen bonding),[13] but also afforded g-C_3N_4 NSs with positively charged surface (zeta-potential: +25.6 mV *vs.* –37.3 mV for pristine g-C_3N_4). Then, the spontaneous assembly between mildly oxidized CNTs (zeta-potential: -19.3 mV) with abundant oxygen-containing functional groups (*e.g.* –COO^-) and positively charged g-C_3N_4 NSs was achieved through a hydrothermal process driven by electrostatic and π-π stacking interactions, forming a 3D composite with numerous pores (see details in Supporting Information and discussion below).

The as-synthesized 2D g-C_3N_4 NSs exhibit an ultrathin layered structure (see scanning electron microscopy (SEM), **Figures S1a, b**, Supporting Information) with negligible amount of bulk domains, indicating high efficiency of the exfoliation process used. The nearly transparent layers reveal the ultrathin thickness (see transmission electron microscopy (TEM), **Figures S1c, d**), consistent with the atomic force microscopy (AFM) observations, which show a thickness of ~3.2 nm, equal to 9–10 CN atomic monolayers (**Figure 1a**). Different from the loosely dispersed g-C_3N_4 NSs, the g-C_3N_4 NS-CNT composite material is assembled by bridging CNTs (**Figure 1b**), as shown in the magnified SEM image (**Figure 1c**), into a 3D porous network composed of thin nanolayers and closely grafted CNTs within the interlayer space. The uniform dispersion of N and C elements in g-C_3N_4 NS-CNT (energy dispersive X-ray spectroscopy (EDS) elemental mapping image, **Figure 1b** insert) verifies a homogeneous distribution of closely interconnected g-C_3N_4 NSs and CNTs (see the TEM image in **Figure 1d**). Thus, microscopy images show a well-connected porous network composed of CNTs coupled with g-C_3N_4 NSs.

It is noteworthy that the characteristic structural features of g-C_3N_4 and CNTs are well preserved in the 3D g-C_3N_4 NS-CNT composite. The presence of g-C_3N_4 domains is verified by two signals in the X-ray diffraction (XRD) pattern (**Figure 1e**), *i.e.* the strong shoulder peak at 2θ of 27.4° (d = 0.326 nm) originated from the (002) interlayer diffraction of a CN graphitic-like structure, and the low-angle diffraction peak at 2θ of 13.3° (d = 0.663 nm) derived from in-planar repeated tri-s-triazine units. Notably, the intensity of these two peaks is sharply reduced as compared to that in the bulk g-C_3N_4 due to the few-layer structure and smaller planar size of NSs after exfoliation.[11,12] The N_2 adsorption isotherm measured for g-C_3N_4 NS-CNT resembles type IV with a H3 type hysteresis loop (**Figure 1f**), confirming the presence of interconnected mesopores. Correspondingly, two peaks centered at 3.3 and 6.5 nm are observed in the pore size distribution curve, which are probably attributed to the inner cavity diameter of CNTs and the pores formed in the assembled 3D matrix, respectively. Besides, g-C_3N_4 NS-CNT exhibits a large surface area of 149 m^2 g^{-1}, consistent with the highly porous structure visible on microscopy observations.

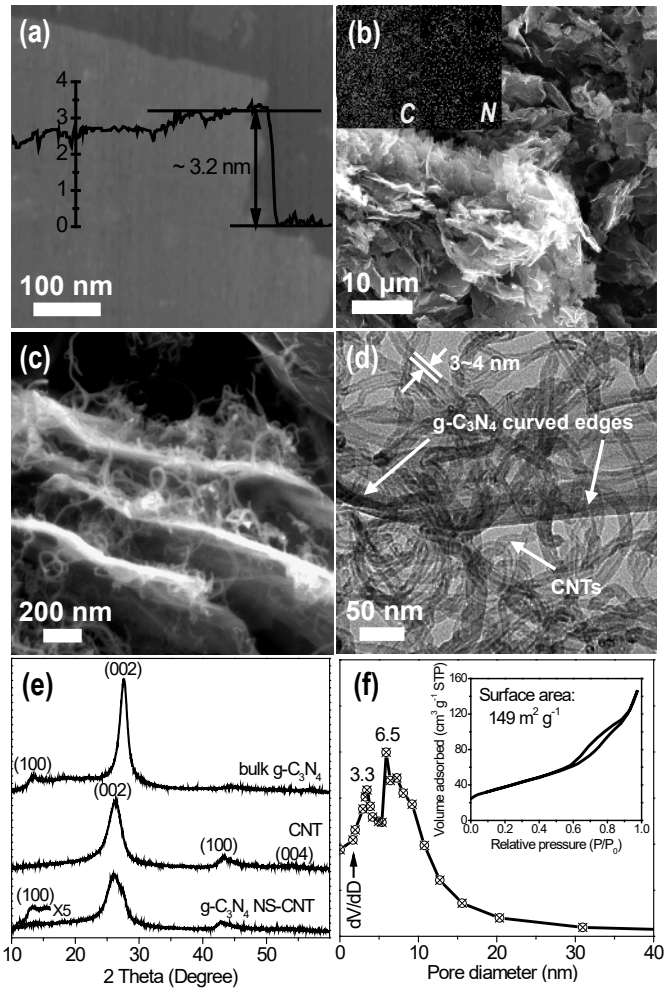

Figure 1. (a) AFM image of g-C_3N_4 NSs. (b, c) SEM, (Inset of b) EDS elemental mapping and (d) TEM images of g-C_3N_4 NS-CNT. (e) XRD patterns of g-C_3N_4 NS-CNT, CNTs and g-C_3N_4. (f) The pore size distribution curve and (inset of f) the N_2 adsorption isotherm recorded for g-C_3N_4 NS-CNT.

A strong coupling between g-C_3N_4 NSs and CNTs in the assembled 3D g-C_3N_4 NS-CNT was firstly confirmed by X-ray photoelectron spectroscopy (XPS), in which both N 1s and C 1s spectra of g-C_3N_4 NS-CNT (**Figure 2**) show distinct profiles as compared to those of g-C_3N_4 (**Figure S2**). Specifically, the best deconvolution of N 1s spectrum was achieved by assumption of four species. The peak at 399.8 eV can be attributed to the bridging N atoms in N(–C)$_3$ or N bonded with H atoms. The dominant peak at 398.3 eV corresponds to the sp^2-bonded N in triazine rings (C–N=C), which splits to form an obvious new shoulder peak at 397.6 eV, caused by the strong interaction between CNTs and N in g-C_3N_4 NSs.[14] Another peak at 403.3 eV is due to the protonation of g-C_3N_4 NSs, which renders CN heterocycles and cyano groups positively charged.[15] The C 1s spectrum of g-C_3N_4 NS-CNT can be deconvoluted into four species, *i.e.* sp^2-bonded C in g-C_3N_4 NSs

(288.0 eV)[11,12] and C=C (284.6 eV), C–OH (285.7 eV), –COOH (289.1 eV) in CNTs.[16] The XPS survey spectrum shows that g-C_3N_4 NS-CNT contains C, N and O with a high N content of 23.7 wt.%, consistent to the elemental analysis result (**Table S1**). Moreover, as seen from Fourier transform infrared (FT-IR) spectra (**Figure S3**), the characteristic bands for the CN heterocycle stretching vibration in g-C_3N_4 NS-CNT show blue-shifts as compared to those in g-C_3N_4, *e.g.* 1390→1371 cm^{-1} and 1538→1522 cm^{-1}, which are also due to the strong interaction between CNTs and g-C_3N_4 NSs. A newborn band centered at ~1730 cm^{-1} is ascribed to the presence of carboxyl groups on the mildly oxidized CNTs.

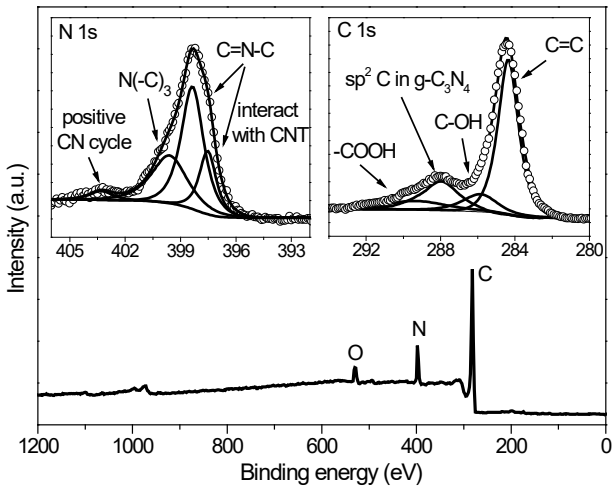

Figure 2. XPS survey and high resolution spectra of N 1s and C 1s core levels in g-C_3N_4 NS-CNT.

The strong coupling between CNTs and g-C_3N_4 NSs proven by microscopy images, XPS and FT-IR is related to the robust self-assembly during the hydrothermal aging process. The driving force for the self-assembly of CNTs and g-C_3N_4 NSs can be attributed to two aspects, *i.e.* the π-π stacking interaction between conjugated tri-s-triazine motifs in g-C_3N_4 NSs and graphene fragments in CNTs, and the electrostatic interaction between $–COO^-$ groups on CNTs (289.1 eV in C 1s XPS; 1730 cm^{-1} in FT-IR) and positively charged g-C_3N_4 NSs (zeta-potential of +25.6 mV; 403.3 eV in N 1s XPS).

The remarkable 3D porous structure composed of strongly coupled CNTs and g-C_3N_4 NSs reveals a great potential of g-C_3N_4 NS-CNT for electrocatalytic oxygen evolution. A slow scan rate (5 mV s^{-1}) was applied during the OER test on a rotating disk electrode (RDE) in alkaline solutions (0.1 M KOH) to minimize the capacitive current. In the linear sweep voltammograms (LSVs, **Figures 3a, S4, S5**), purified oxidized CNTs and g-C_3N_4 NSs show negligible OER response, indicating that the trace metal residues in CNTs (see details in Supporting Information) hardly contribute to the catalytic OER activity. The anodic current recorded on g-C_3N_4 NS-CNT renders a sharp onset potential at ~1.53 V, declaring the coupling of two components can significantly improve the catalytic activity. IrO_2-CNT affords a slightly lower onset potential (~1.51 V), but its OER current density drops below that of g-C_3N_4 NS-CNT at the potential higher than 1.62 V, featuring the better performance of g-C_3N_4 NS-CNT.

The operating potentials (*vs.* RHE) to deliver a 10 mA cm^{-2} current density were compared, which is expected for a 10% efficient solar water-splitting device.[17] 3D g-C_3N_4 NS-CNT generates a current density of 10 mA cm^{-2} at 1.60 V, similar to that of IrO_2-CNT (1.59 V), and comparable to that of the state-of-the-art noble-metal catalysts, *e.g.* IrO_2/C (1.60 V, 0.1 M KOH),[6] colloidal IrO_2 nanoparticles (1.60 V, 0.5 M H_2SO_4),[18] $Ru_{0.2}Ir_{0.8}O_2$ (1.61 V, 0.5 M H_2SO_4)[19] and transition metal catalysts, *e.g.* Mn_3O_4/$CoSe_2$ hybrids (1.68 V, 0.1 M KOH),[20] Co_3O_4/N-graphene (1.63 V, 1 M KOH).[3d] The activity of g-C_3N_4 NS-CNT is also higher than previously reported N(5)-ethylflavinium ions[4] and N-doped graphene/CNT composites (> 1.65 V, 0.1 M KOH).[5]

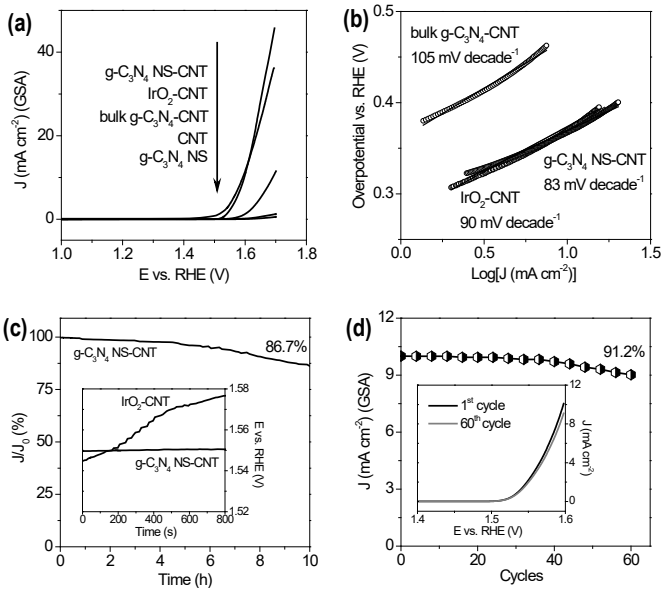

Figure 3. (a) LSVs and (b) Tafel plots of g-C_3N_4 NS-CNT, IrO_2-CNT, bulk g-C_3N_4-CNT, purified oxidized CNTs and g-C_3N_4 NSs on a RDE (1500 rpm) in an O_2-saturated 0.1 M KOH solution (scan rate: 5 mV s^{-1}). The calculation of the OER current density was based on the geometric surface area (GSA).[2,3] (c) Chronoamperometric response at a constant potential of 1.54 V, and (inset of c) chronopotentiometric response of g-C_3N_4 NS-CNT as compared to IrO_2-CNT at a constant current density of 3.0 mA cm^{-2}. (d) A curve of the current density of g-C_3N_4 NS-CNT at 1.60 V *vs.* scan cycles, and (inset of d) LSVs of g-C_3N_4 NS-CNT before and after 60 scan cycles (scan rate: 5 mV s^{-1}).

The catalytic kinetics for oxygen evolution was examined by Tafel plots (**Figure 3b**). The lower Tafel slope value of g-C_3N_4 NS-CNT (83 mV $decade^{-1}$) indicates its more favorable kinetics in comparison to that of IrO_2-CNT (90 mV $decade^{-1}$). This result well agrees with the higher catalytic current density of g-C_3N_4 NS-CNT than that of IrO_2-CNT at high potential region (> 1.62 V) (**Figures 3a, S6**), suggesting better catalytic activity of g-C_3N_4 NS-CNT.

The chronoamperometric response demonstrates the high stability of g-C_3N_4 NS-CNT, showing slight anodic current attenuation of 13.3% within 10 hours (**Figures 3c, S7**). The insignificant activity decrease may be ascribed to the mass loss of catalysts on the electrode, because a large amount of oxygen is evolved through the porous system of catalysts, causing the partial peeling off of the coated layer. Also, in the chronopotentiometric response, g-C_3N_4 NS-CNT displays a nearly constant operating potential at 1.55 V to deliver a 3.0 mA cm^{-2} current density (**Figure 3c** inset), whereas the potential of IrO_2-CNT shows an increase of ~32 mV within 800 s, revealing g-C_3N_4 NS-CNT has higher stability than IrO_2-CNT. Further, 91.2% of the original catalytic current can be remained after 60 scan cycles at a scan rate of 5 mV s^{-1} (**Figure 3d**). The smooth performance in high-concentration alkaline solutions is critical for realistic applications.[17] In 1 M KOH, the high activity of g-C_3N_4 NS-CNT is well preserved with a sharp onset potential of 1.47 V, and the chronopotentiometric response shows its operating potential stable at ~1.48 V to deliver a 2.0 mA cm^{-2} current density (**Figure S8**), which corroborates the effective operation of g-C_3N_4 NS-CNT in concentrated electrolytes.

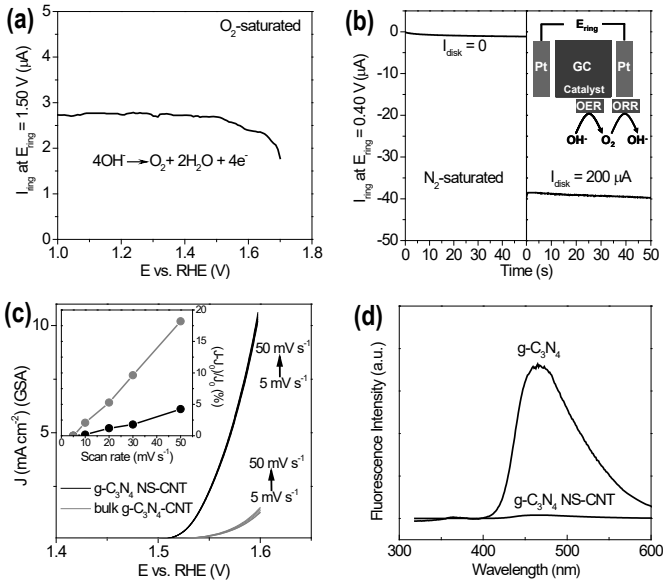

Figure 4. (a) The ring current of g-C_3N_4 NS-CNT on a RRDE (1500 rpm) in O_2-saturated 0.1 M KOH solution (ring potential: 1.50 V). (b) The ring current of g-C_3N_4 NS-CNT on a RRDE (1500 rpm) in N_2-saturated 0.1 M KOH solution (ring potential: 0.40 V). (c) LSVs of g-C_3N_4 NS-CNT and bulk g-C_3N_4-CNT at different scan rates and (inset of c) the corresponding data replotted as the current density (at 1.60 V) increased percentage *vs.* scan rates. (d) Fluorescence emission spectra of g-C_3N_4 NS-CNT and g-C_3N_4.

To gain insight into the reaction mechanism, the rotating ring-disk electrode (RRDE) technique was employed with a Pt ring electrode potential of 1.50 V to detect the peroxide species formed at the g-C_3N_4 NS-CNT catalyst surface during OER. A very low ring current (μA scale) was recorded (**Figure 4a**), which is three orders of magnitude lower than that of the disk current (mA scale), suggesting almost no formation of hydrogen peroxide. This result indicates that g-C_3N_4 NS-CNT favors a desirable four-electron water oxidation pathway. To ensure the observed oxidation current is from oxygen evolution, a RRDE in N_2-saturated 0.1 M KOH solution was applied. With the disk current at 200 μA, O_2 molecules generated from the catalyst on the disk sweep across the surrounding Pt ring held at an ORR potential of 0.40 V, and are rapidly reduced (**Figure 4b**). Thus, a ring current of ~40 μA (200 μA × 0.2, RRDE collecting efficiency = 0.2) was detected, which suggests the observed oxidation current can be fully related to OER. Accordingly, the Faradaic efficiency of g-C_3N_4 NS-CNT is calculated to be ~ 99.2%.

The outstanding OER activity of g-C_3N_4 NS-CNT originates from its high N content (active site concentration), unique porous architecture (mass transport) and strong coupling between g-C_3N_4 NSs and CNTs (electron conductivity). Firstly, the g-C_3N_4 NS-CNT catalyst features a high N content of 23.7 wt.%, which surpasses that of the most N-doped carbon catalysts reported,[7a,b,d,10] because the new low-temperature synthesis affords strong coupling between g-C_3N_4 NSs and CNTs. The extensively present electron-accepting pyridinic and tertiary N species can impart a relatively high positive charge density on the neighboring sp^2-bonded C atoms.[7a] According to the OER pathway in alkaline solutions ($4OH^- \rightarrow O_2 + 2H_2O + 4e^-$), the positive carbon atoms can facilitate adsorption of OH^-, promote the electron transfer between the catalyst surface and reaction intermediates (*e.g.* O^{2-}), and assure an easy recombination of two adsorbed oxygen atoms for O_2 evolution.[21]

Secondly, to illustrate the importance of porous 3D structure, the bulk g-C_3N_4-CNT was prepared for the purpose of comparison by coupling CNTs with bulk g-C_3N_4 instead of g-C_3N_4 NSs (see details in Supporting Information), which resulted in a non-porous structure with a low surface area of 32 m^2 g^{-1} (**Figure S9**). Bulk g-C_3N_4-CNT shows low OER activity and unfavorable kinetics as compared to g-C_3N_4 NS-CNT (**Figure 3**), and its current density is more susceptible to the scan rate, showing a variation of 18.7% (*vs.* 4.8 % of g-C_3N_4 NS-CNT) with increasing the scan rate from 5 mV s^{-1} to 50 mV s^{-1} (**Figure 4c**), due to the restricted mass transfer in the nonporous solid. These facts demonstrate the significant importance of highly porous 3D architecture in g-C_3N_4 NS-CNT, which favors the easy infiltration of electrolytes, the efficient transfer of reactants (*i.e.* OH^-), as well as the fast emission of products (*i.e.* O_2).

Thirdly, the poor electron transfer in g-C_3N_4 is the primary barrier for its electrocatalytic applications,[7b,c,d,8] which is conquered herein by strong coupling of highly conductive CNTs with semiconducting g-C_3N_4 (as evidenced by microscopy images, XPS and FT-IR). The smooth transfer of the generated catalytic current through the π-π stacking between g-C_3N_4 NSs and CNTs is proven by fluorescence emission spectra (**Figure 4d**). As compared to the high fluorescence intensity of g-C_3N_4, the fluorescence is completely quenched in g-C_3N_4 NS-CNT, indicating the photo-generated electrons on g-C_3N_4 NSs can be easily transferred to CNTs. In contrast, the inferior interaction and electron transport between bulk g-C_3N_4 and CNTs in the bulk g-C_3N_4-CNT catalyst is another reason responsible for its low OER activity besides the limited mass transfer. Due to the aforementioned three advantages, a series of 3D composites with different g-C_3N_4 NS/CNT ratios was synthesized with the high catalytic activity for OER (**Figures S10, S11, Table S1**).

In summary, 3D g-C_3N_4 NS-CNT porous composites are reported to exhibit the highest activity among non-metal OER catalysts, and better performance with more favorable kinetics and stronger durability than Ir-based noble-metal OER catalysts. Their outstanding activity can be attributed to the large amount of active sites related to the high N concentration, and the improved charge and mass transport ability due to the 3D interconnected porous framework. Further effort will be made on fabricating self-supported electrodes to increase the long-term stability and replacing CNTs with other low-price carbon supports to reduce the cost.

Received: ((will be filled in by the editorial staff))
Published online on ((will be filled in by the editorial staff))

Keywords: carbon nitride nanosheet • carbon nanotube • oxygen evolution • electrocatalysis • porous structure

[1] a) T. Ogasawara, A. Débart, M. Holzapfel, P. G. Bruce, *J. Am. Chem. Soc.* **2006**, *128*, 1390–1393; b) N. S. Lewis, *Science* **2007**, *315*, 798−801; c) R. F. Service, *Science* **2009**, *324*, 1257–1259.

[2] a) M. G. Walter, E. L. Warren, J. R. McKone, S. W. Boettcher, Q. Mi, E. A. Santori, N. S. Lewis, *Chem. Rev.* **2010**, *110*, 6446−6473; b) Y. Lee, J. Suntivich, K. J. May, E. E. Perry, Y. Shao-Horn, *J. Phys. Chem. Lett.* **2012**, *3*, 399−404.

[3] a) W. C. Ellis, N. D. McDaniel, S. Bernhard, T. J. Collins, *J. Am. Chem. Soc.* **2010**, *132*, 10990–10991; b) Q. Yin, J. M. Tan, C. Besson, Y. V. Geletii, D. G. Musaev, A. E. Kuznetsov, Z. Luo, K. I. Hardcastle, C. L. Hill, *Science* **2010**, *328*, 342–345; c) J. Suntivich, K. J. May, H. A. Gasteiger, J. B. Goodenough, Y. Shao-Horn, *Science* **2011**, *334*, 1383−1385; d) Y. Liang, Y. G. Li, H. L. Wang, J. G. Zhou, J. Wang, T. Regier, H. J. Dai, *Nat. Mater.* **2011**, *10*, 780−786.

[4] E. Mirzakulova, R. Khatmullin, J. Walpita, T. Corrigan, N. M. Vargas-Barbosa, S. Vyas, S. Oottikkal, S. F. Manzer, C. M. Hadad, K. D. Glusac, *Nat. Chem.* **2012**, *4*, 794–801.

[5] a) S. Chen, J. J. Duan, M. Jaroniec, S. Z. Qiao, *Adv. Mater.* **2014**, DOI: 10.1002/adma.201305608; b) H. W. Park, D. U. Lee, Y. Liu, J. Wu, L. F. Nazar, Z. Chen, *J. Electrochem. Soc.* **2013**, *160*, A2244–A2250.

[6] Y. Zhao, R. Nakamura, K. Kamiya, S. Nakanishi, K. Has himoto, *Nat. Commun.* **2013**, *4*, 2390.

[7] a) K. Gong, F. Du, Z. Xia, M. Durstock, L. Dai, *Science* **2009**, *323*, 760–764; b) Y. Zheng, Y. Jiao, J. Chen, J. Liu, J. Liang, A. Du, W. Zhang, Z. Zhu, S. C. Smith, M. Jaroniec, G. Q. Lu, S. Z. Qiao, *J. Am. Chem. Soc.* **2011**, *133*, 20116–20119; c) Y. Zheng, Y. Jiao, Y. Jin, M. Jaroniec, S. Z. Qiao, *Small* **2012**, *8*, 3550–3566; d) J. Liang, Y. Zheng, J. Chen, J. Liu, D. Hulicova-Jurcakova, M. Jaroniec, S. Z. Qiao, *Angew. Chem.* **2012**, *124,* 3958–3962; *Angew. Chem. Int. Ed.* **2012**, *51,* 3892–3896.

[8] a) A. Thomas, A. Fischer, F. Goettmann, M. Antonietti, J. O. Müller, R. Schlögl, J. M. Carlsson, *J. Mater. Chem.* **2008**, *18*, 4893–4908; b) Y. Wang, X. Wang, M. Antonietti, *Angew. Chem.* **2012**, *124*, 70–92; *Angew. Chem. Int. Ed.* **2012**, *51*, 68–89.

[9] S. M. Lyth, Y. Nabae, S. Moriya, S. Kuroki, M. Kakimoto, J. Ozaki, S. Miyata, *J. Phys. Chem. C* **2009**, *113*, 20148–20151.

[10] a) S. M. Lyth, Y. Nabae, N. M. Islam, S. Kuroki, M. Kakimoto, S. Miyata, *J. Electroanal. Chem.* **2011**, *158*, B194–B201; b) S. Yang, X. Feng, X. Wang, K. Müllen, *Angew. Chem.* **2011**, *123*, 5451–5455; *Angew. Chem. Int. Ed.* **2011**, *50*, 5339–5343; c) Y. Sun, C. Li, Y. Xu, H. Bai, Z. Yao, G. Shi, *Chem. Commun.* **2010**, *46*, 4740–4742.

[11] P. Niu, L. Zhang, G. Liu, H. M. Cheng, *Adv. Funct. Mater.* **2012**, *22*, 4763–4770.

[12] a) X. Zhang, X. Xie, H. Wang, J. Zhang, B. Pan, Y. Xie, *J. Am. Chem. Soc.* **2013**, *135*, 18–21; b) J. Tian, Q. Liu, A. M. Asiri, A. O. Al-Youbi, X. Sun, *Anal. Chem.* **2013**, *85*, 5595–5599; c) S. Yang, Y. Gong, J. Zhang, L. Zhan, L. Ma, Z. Fang, R. Vajtai, X. Wang, P. M. Ajayan, *Adv. Mater.* **2013**, *25*, 2452–2456.

[13] a) B. V. Lotsch, M. Doblinger, J. Sehnert, L. Seyfarth, J. Senker, O. Oeckler, W. Schnick, *Chem. Eur. J.* **2007**, *13*, 4969–4980; b) J. N. Coleman, *Accounts Chem. Res.* **2013**, *46*, 14–22; c) T. Y. Ma, Y. H. Tang, S. Dai, S. Z. Qiao, *Small* **2014**, DOI: 10.1002/smll.201303827.

[14] Q. Liu, J. Zhang, *Langmuir* **2013**, *29*, 3821–3828.

[15] a) D. Foy, *J. Solid State Chem.* **2009**, *182*, 165–171; b) R. C. Dante, P. Martin-Ramos, A. Correa-Guimaraes, J. Martin-Gil, *Mater. Chem. Phys.* **2011**, *130*, 1094–1102.

[16] Y. Zheng, Y. Jiao, L. Ge, M. Jaroniec, S. Z. Qiao, *Angew. Chem.* **2013**, *125*, 3192−3198; *Angew. Chem. Int. Ed.* **2013**, *52*, 3110−3116.

[17] C. C. L. McCrory, S. Jung, J. C. Peters, T. F. Jaramillo, *J. Am. Chem. Soc.* **2013**, *135*, 16977–16987.

[18] W. Hu, Y. Wang, X. Hu, Y. Zhou, S. Chen, *J. Mater. Chem.* **2012**, *22*, 6010–6016.

[19] N. Mamaca, E. Mayousse, S. Arrii-Clacens, T. W. Napporn, K. Servat, N. Guillet, K. B. Kokoh, *Appl. Catal. B: Environ.* **2012**, *111–112*, 376–380.

[20] M. R. Gao, Y. F. Xu, J. Jiang, Y. R. Zheng, S. H. Yu, *J. Am. Chem. Soc.* **2012**, *134*, 2930–2933.

[21] a) R. Cao, J. S. Lee, M. Liu, J. Cho, *Adv. Energy Mater.* **2012**, *2*, 816–829; b) H. Wang, H. Dai, *Chem. Soc. Rev.* **2013**, *42*, 3088–3113.

Oxygen Evolution

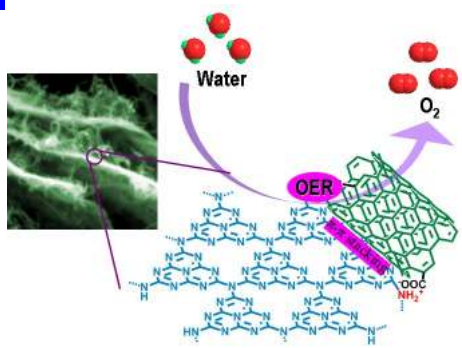

Highly active OER catalysts: 3D porous g-C_3N_4 nanosheet-CNT composites are synthesized through a spontaneous assembly process. The high nitrogen content, enhanced electron conductivity and improved mass transport result in their excellent catalytic oxygen evolution activity and strong durability, superior to those reported for other non-metal catalysts and noble metal catalysts (see picture).